Storage of X-ray photons in a crystal resonator

K.-D. Liss*, R. Hock†, M. Gomm†, B. Waibel‡, A. Magerl†, M. Krisch* & R. Tucoulou*

* *European Synchrotron Radiation Facility, B.P. 220, F-38043 Grenoble Cedex, France*
† *Lehrstuhl fur Kristallographie und Strukturphysik, D-91054 Erlangen, Germany*
‡ *MTU (Motoren- und Turbinen-Union) GmbH, D-80991 München, Germany*

The temporal structure and high brilliance of the X-ray beams produced by third-generation synchrotrons open up new possibilities in time-dependent diffraction and spectroscopy, where timescales down to the sub-nanosecond regime can now be accessed. These beam properties are such that one can envisage the development of the X-ray equivalent of optical components, such as photon delay lines and resonators, that have proved indispensable in a wide range of experiments—for example, pump-probe and multiple-interaction experiments—and (through shaping the temporal structure and repetition rate of the beams) time-dependent measurements in crystallography, physics, biology and chemistry[1–3]. Optical resonators, such as those used in lasers, are available at wavelengths from the visible to soft X-rays[4,5]. Equivalent components for hard X-rays have been discussed for more than thirty years[4,6,7], but have yet to be realized. Here we report the storage of hard X-ray photons (energy 15.817 keV) in a crystal resonator formed by two plates of crystalline silicon. The photons are stored for as many as 14 back-and-forth cycles within the resonator, each cycle separated by one nanosecond.

The X-ray resonator consists of a pair of vertical plates cut from a monolithic silicon crystal, separated by 150 mm and with the 111 orientation along their surface normals, as sketched in Fig. 1. The plates are slightly wedge-shaped in order to vary the effective crystal thickness between 50 μm and 500 μm by a horizontal translation perpendicular to the axis of the beam. The experiment was performed at the inelastic scattering beamline ID28 at the European Synchrotron Radiation Facility (ESRF). The radiation from the undulator source was monochromatized using the silicon 888 reflection at a Bragg angle of 89.865 degrees. This provided an X-ray beam of approximately 15.817 keV with an energy resolution of 3.7 meV and a divergence of about 10 mrad. The energy of the incoming photons could be varied through thermal expansion of the lattice spacing by an accurate temperature control of the monochromator, and a typical overall stability of 10 mK during the integration time of one pattern could be achieved. (Using the thermal expansion coefficient $\alpha = 2.56 \times 10^{-6}\ \mathrm{K}^{-1}$ for silicon, gives the relative lattice parameter uncertainty $\Delta d/d = \alpha \Delta T = 2.56 \times 10^{-8}$, where T is temperature. This is a much smaller value than the energy resolution $\Delta E/E = 2.3 \times 10^{-7}$ of the incident X-ray beam.) The resonator was aligned such that photons are Bragg reflected exactly back into the axis of the incident beam, and the intensity transmitted through the crystal plates was measured behind the resonator by a fast avalanche diode with a response time matching the intrinsic time structure of the synchrotron X-ray beam.

The Bragg condition for the resonator was determined by energy variation of the incoming photons through the controlled thermal expansion of the monochromator lattice spacing. The result of such a scan is shown in Fig. 2. The exact Bragg condition is fulfilled when the transmitted intensity has a minimum, because most of the photons are then back reflected and do not reach the detector. The observed full-width-half-maximum (FWHM) on the relative energy scale is $\Delta E/E = 7.4 \times 10^{-7}$ and the minimum transmission through the two 292-μm slices is 17% after consideration of normal absorption.

Figure 1 Sketch of the resonator with the two active slices sticking out of the monolithic device. Photons impinging from the left can be trapped due to transmission and reflection probabilities T and R, respectively. They exit the resonator with probabilities TT, $TRRT$, $TRRRRT\ldots T^2R^{2N}$ for 0, 1, 2…N back-and-forth bounces at t_0, t_1…, being delayed by N times the time of flight inside the resonator of 1.0 ns. The reflection angle is adjusted to exactly 180 degrees and the beam paths of multiply reflected photons are exactly superimposed in space.

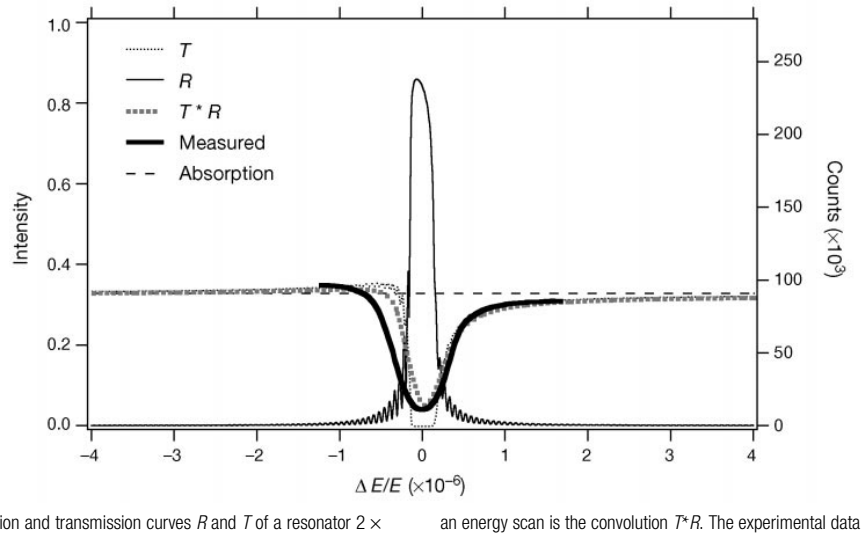

Figure 2 Calculated reflection and transmission curves R and T of a resonator 2 × 292 μm in thickness as a function of relative energy deviation $\Delta E/E$ from the centre of the Bragg reflection. The monochromator delivers a similar curve to R, regardless of the small wiggles stemming from the slice thickness; thus the calculated curve for the simulation of an energy scan is the convolution $T*R$. The experimental data have been adapted to the intensity scale. The dashed line is the absorption far off the Bragg peak; the experimental data is consistent with theory for anomalous absorption, the asymmetry around the Bragg position.

The time dependence of the transmitted beam at the centre of the Bragg reflection, that is, at the dip in Fig. 2, is shown in Fig. 3 for various crystal thicknesses. The data was obtained in the ESRF 16-bunch mode where X-ray pulses of 100-ps duration are separated by 176 ns. The time delay between a registered photon and the synchrotron bunch clock was measured stroboscopically and the events were stored in corresponding channels of a multi-channel analyser[3]. The first curve shows the time structure of the detector without the resonator in the beam. The intensity maximum corresponds to the undelayed photons at time $t = 0$. The signal has a FWHM of 500 ps, corresponding to the time response of the detector. The shape asymmetry arises from intrinsic capacities[8] and can be neglected in this experiment. The time patterns with the resonator in the Bragg position differ qualitatively from the first curve and show a series of sequential maxima separated by 1.0 ns forming an exponential decay towards longer times. The maxima correspond to photons trapped within the resonator for 1, 2, 3…N successive reflections from both crystal plates. When the beam impinges onto the first crystal slice, there is a probability for transmission, giving the forward diffracted beam. The same holds for the second plate and therefore yields a maximum signal at $t = 0$. But there is also a probability for reflection at each slice, permitting part of the beam to go back and forth and thus travel several times the length between the slices, that is, multiples of 30 cm in length or of 1.0 ns in time, resulting in the detected peak separations. We observe up to 14 peaks corresponding to up to 14.0 ns of time delay and even intensity beyond that for the 243-μm-thick crystals. The delayed maxima are less intense for thicker crystal slices because the transmission probability for entering and leaving the resonator is reduced, even in the case of no absorption, and a compromise has to be made between transmission and reflectivity.

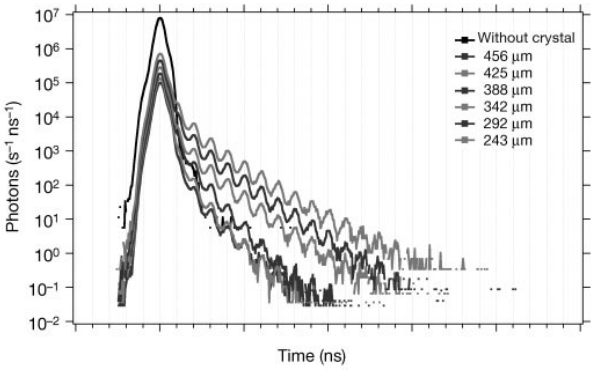

Figure 3 Time pattern of stored photons at the exit of the resonator. Without the crystal in the beam, only a direct bunch of photons is observed at time zero, whereas many bunches appear when the device is in Bragg condition. Each peak at later times corresponds to multiple back-and-forth travels inside the device. The widths of the peaks are dominated by the time resolution of the avalanche detector.

The storage capacity of the resonator depends on the ratio of the crystal thickness to the 'Pendellösung period' of the chosen reflection[9]; this ratio defines the minimum thickness that will yield maximum reflectivity. For the silicon 888 reflection it is 150 μm; a resonator of this plate thickness would reach optimum storage and thus longest delay times. For thicker crystals, fewer photons enter or exit the resonator, as a result of back reflection, and so the total observed intensity decreases. Thinner crystals down to half a Pendellösung period could be useful for a small number of bounces, that is, a small number of reflections, when higher transmission is advantageous at the cost of reduced reflectivity.

The intensity ratios between successive back-and-forth bounces derived from Fig. 3 are plotted in Fig. 4 as a function of the number of bounces. Again, the thinnest crystal gives the highest values. Most of the intensity leaks out of the resonator during the first bounces, mainly as photons with energies in the tails of the reflection curve where the reflectivity is low. Photons exactly fulfilling the Bragg condition have the highest reflectivity and thus survive longest in the cavity. Consequently, the beam becomes first highly monochromatic, reducing the intensity of its wings, and only photons in a very narrow energy range within the intrinsic width of the reflection curve remain in the resonator. The experimental bounce ratio approaches asymptotically the value 0.5, corresponding to a crystal reflectivity of about 70%. The points connected by the continuous line are results from a calculation. The curve shows a faster decrease for the very first bounces followed by a higher asymptotic value of 66%. These discrepancies with theory are consistent with the broader width and deeper dip in the experimental energy scan of Fig. 2 and are probably attributable to lattice strain of the Czochralski grown crystal with high oxygen concentration used in this set-up.

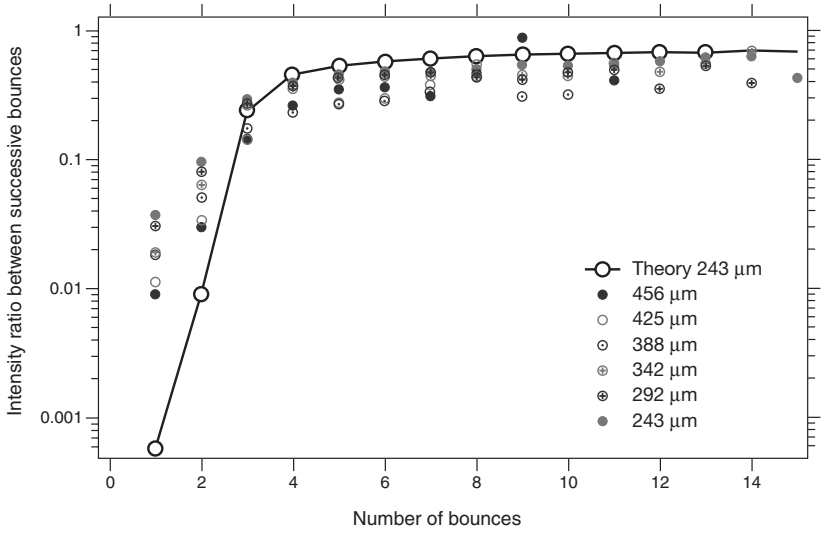

Figure 4 Intensity ratios between neighbouring peaks in the time period of Fig. 3 and calculated values obtained from dynamical theory (joined circles).

In the present set-up, photons are stored by reflections from two independent Bragg mirrors, that is, the photon pulse length is shorter than the resonator length. We envisage the construction of a Fabry–Perot-type interferometer where the incoming beam would interfere coherently with both crystal slabs. This additional interference would lead to a transmission resonance at least ten times sharper than the natural Bragg line width. Such devices necessitate a gap width of a few Pendellösung periods, that is, a few hundred micrometres (refs 10 and 11). With the development of free electron lasers, pulses on the 100-fs scale will become available–matching these distances perfectly. □

Received 7 September 1999; accepted 20 January 2000.

1. Perman, B. *et al.* Energy transduction on the nanosecond time scale: early structural events in a xanthopsin photocycle. *Science* **279,** 1946–1950 (1998).
2. Rose-Petruck, C. *et al.* Picosecond-milliAngstrom lattice dynamics measured by ultrafast X-ray diffraction. *Nature* **398,** 310–312 (1999).
3. Liss, K. -D., Magerl, A., Hock, R., Waibel, B. & Remhof, A. The investigation of ultrasonic fields by time resolved X-ray diffraction. *Proc. SPIE* **3451,** 117–127 (1998).
4. Bond, W. L., Duguay, M. A. & Rentzepis, P. M. Proposed resonator for an X-ray laser. *Appl. Phys. Lett.* **10,** 216–218 (1967).
5. Ceglio, N. M., Gaines, D. P., Trebes, J. E., London, R. A. & Stearns, D. G. Time-resolved measurement of double pass amplification of soft X-rays. *Appl. Opt.* **27,** 5022–5025 (1988).
6. Deslattes, R. D. X-ray monochromators and resonators from single crystals. *Appl. Phys. Lett.* **12,** 133–135 (1968).
7. Hart, M. Bragg reflection X-ray optics. *Rep. Prog. Phys.* **34,** 435–490 (1971).
8. Kishimoto, S. An avalanche photodiode detector for X-ray timing measurements. *Nucl. Instrum. Methods Phys. Res. A* **309,** 603–605 (1991).
9. Zachariasen, W. H. *Theory of X-Ray diffraction in Crystals* (Wiley, London, 1945).
10. Steyerl, A. & Steinhauser, K.-A. Proposal of a Fabry-Perot-type interferometer for X-rays. *Z. Phys. B* **34, 221–227 (1979).**
11. Caticha, A. & Caticha-Ellis, S. A Fabry-Perot interferometer for hard X-rays. *Phys. Status Solidi A* **119,** 643–654 (1990).

Acknowledgements

We thank the European Synchrotron Radiation Facility crystal laboratory for the preparation of the resonator.

Correspondence and requests for materials should be addressed to K.-D.L. (e-mail: liss@esrf.fr).